

Visualizing Head and Neck Tumors In Vivo Using Near-Infrared Fluorescent Transferrin Conjugate

Liang Shan, Yubin Hao, Songping Wang, Alexandru Korotcov, Renshu Zhang, Tongxin Wang, Joseph Califano, Xinbin Gu, Rajagopalan Sridhar, Zaver M. Bhujwalla, and Paul C. Wang

Abstract

Transferrin receptor (TfR) is overexpressed in human head and neck squamous cell carcinomas (HNSCCs). This study was carried out to investigate the feasibility of imaging HNSCC by targeting TfR using near-infrared fluorescent transferrin conjugate (Tf^{NIR}). Western blot analysis of four HNSCC cell lines revealed overexpression of TfR in all four lines compared with that in normal keratinocytes (OKFL). Immunocytochemistry further confirmed the expression of TfR and endocytosis of Tf^{NIR} in JHU-013 culture cells. Following intravenous administration of Tf^{NIR} (200 μ L, 0.625 μ g/ μ L), fluorescent signal was preferentially accumulated in JHU-013 tumor xenografts grown in the lower back ($n = 14$) and oral base tissues ($n = 4$) of nude mice. The signal in tumors was clearly detectable as early as 10 minutes and reached the maximum at 90 to 120 minutes postinjection. The background showed an increase, followed by a decrease at a much faster pace than tumor signal. A high fluorescent ratio of the tumor to muscle was obtained (from 1.42 to 4.15 among tumors), usually achieved within 6 hours, and correlated with the tumor size ($r = .74$, $p = .002$). Our results indicate that TfR is a promising target and that Tf^{NIR}-based optical imaging is potentially useful for noninvasive detection of early HNSCC in the clinic.

A CHALLENGE IN NEOPLASTIC DIAGNOSTICS is noninvasive detection of tumors at an early stage and providing information on treatment selection and its outcome. Molecular imaging provides opportunities to fulfill the clinical needs.^{1–3} Its advancement benefits from the identification of hundreds of biomarkers that are highly expressed in tumors.^{4,5} In theory, by detecting the differences in “molecular properties” between cancer and surrounding normal tissues, the signal to noise ratio can be significantly increased, and that should allow for detection of smaller tumors. Relative to other imaging techniques, near-infrared (NIR) fluorescence-based optical imaging

offers unique advantages for diagnostic imaging of solid tumors. Newly developed fluorescent contrast agents and highly sensitive light detection systems have made it possible to monitor the biologic activity of a wide variety of molecular targets, such as intracellular enzymes, cell surface receptors, and antigens in living subjects. NIR optical imaging is highly sensitive, with a capability to detect a molecular probe at 10^{-9} to 10^{-12} mol/L without much interference from background and does not require the use of radioactive materials.¹ Because water and biologic tissues have minimal absorbance and autofluorescence in the NIR window (650–980 nm), efficient photon penetration into and out of tissue with low intratissue scattering can be achieved with a depth of about 1 cm for reflectance and 2 to 6 cm for tomographic fluorescence.^{1,6} Although clinical application of optical imaging is limited owing to poor tissue penetration, the notable theoretical advantages include imaging a variety of molecular features based on versatile fluorescent probe design, providing dynamic, real-time in vivo images, monitoring of gene delivery, noninvasive detection of early tumors from accessible lumina by endoscopy, and real-time intraoperative visualization of tumor margins.^{7,8}

In the United States, more than 55,000 Americans develop head and neck cancer each year. Squamous cell carcinoma accounts for 90% of the head and neck

From the Departments of Radiology, Oral Diagnostic Service, and Radiation Oncology, Howard University, Washington, DC, and Departments of Otolaryngology and Radiology, Johns Hopkins University, Baltimore, MD.

This work was supported in part by Department of Defense grant USAMRMC W81XWH-05-1-0291, the Charles and Mary Latham Fund (7023185), and National Institutes of Health National Center for Research Resources/Research Centers in Minority Institutions Program grants 2G12 RR003048, 5P20 CA118770, and 5U 54CA091431.

Address reprint requests to: Paul C. Wang, PhD, Department of Radiology, Howard University, 2041 Georgia Avenue, NW, Washington, DC 20060; e-mail: pwang@howard.edu.

DOI 10.2310/7290.2008.0006

© 2008 BC Decker Inc

cancers.⁹ Head and neck squamous cell cancer (HNSCC) develops through a series of well-defined clinical and pathologic stages from atypia to carcinoma in situ and invasive lesions.^{10,11} These lesions locate superficially, which makes them ideal for early detection and evaluation of biomarker expression using optical imaging. Transferrin receptor (TfR) is a cell-membrane internalizing receptor that is responsible for almost all of the iron sequestration in mammalian cells. It is overexpressed in various malignant tumors.^{12–14} Previous work using radiolabeled transferrin (Tf) has demonstrated the feasibility of imaging mammary gland tumor xenografts with high sensitivity.^{15,16} However, targeted detection methods based on radiolabeled probes have been hampered by relatively low spatial resolution and the risk of ionizing radiation exposure. Positron emission tomography (PET) involves the generation of positron-emitting short-lived radioisotopes using a cyclotron. This limits the accessibility of PET in many locations. There are also problems associated with the time necessary for conjugating a short-lived positron emitter to biomolecules. We hypothesized that TfR would be a promising target and NIR fluorescent Tf conjugate (Tf^{NIR}) would be an ideal optical reporter for imaging HNSCC because TfR is expressed only in the parabasal and basal layers of normal squamous epithelium at a very low level and rarely in benign lesions. Importantly, TfR is overexpressed in the majority of HNSCC.^{17–19} Since HNSCCs are superficial tumors, they are ideal for early detection and evaluation of biomarker expression using optical imaging. In the present study, we investigated the feasibility of imaging HNSCC xenografts using Tf^{NIR}. A preferential accumulation of fluorescent signal was observed in tumors, and the tumor was clearly detectable in Tf^{NIR}-based optical imaging.

Materials and Methods

Cell Culture

Four HNSCC cell lines (John Hopkins University, Baltimore, MD) were analyzed for TfR expression. These cell lines were originally established from human HNSCC arising from the base of the tongue (JHU-06), larynx (JHU-011 and 022), and neck node (JHU-013) metastasis. All four cell lines were routinely maintained in RPMI 1640 medium supplemented with 10% heat-inactivated fetal bovine serum and 50 µg/mL each of penicillin, streptomycin, and neomycin (Invitrogen, Carlsbad, CA). A normal human keratinocyte line (OKFL) was used as a control and cultured in keratinocyte serum-free medium (Invitrogen, Carlsbad, CA).²⁰

Western Blot Analysis

Cells were washed twice with Dulbecco's phosphate buffered saline (DPBS) and collected in protein lysis buffer containing 50 mM Tris (pH 8.0), 150 mM NaCl, 0.1% sodium dodecyl sulfate (SDS), 0.5% sodium deoxycholate, 1% NP40, 100 µg/mL of phenylmethylsulfonyl fluoride, 2 µg/mL of aprotinin, 1 µg/mL of pepstatin, and 10 µg/mL of leupeptin. The mixture was placed on ice for 30 minutes. Following centrifugation at 15,000 rpm for 15 minutes at 4°C, the supernatant was collected. Protein concentration was determined using the Bio-Rad Protein Assay Dye Reagent Concentrate (Bio-Rad, Hercules, CA). Whole-cell lysate (30 µg) was resolved in 8% SDS-polyacrylamide gel, transferred to polyvinylidene difluoride membrane (Immobilon, Amersham Corp., Arlington Heights, IL), and probed sequentially with antibodies against TfR (Invitrogen) and β-actin (Sigma, St. Louis, MO) at 4°C overnight, separately. Blots were washed thrice (10 minutes each) with PBS + 0.1% Tween 20 and incubated with horseradish peroxidase-conjugated anti-mouse antibody (Santa Cruz Biotech, Santa Cruz, CA) for 1 hour at room temperature. Blots were developed using the ECL detection system (Bio-Rad).

Endocytosis of Tf and Immunocytochemistry of TfR

JHU-013 tumor cells at 40 to 50% confluence growing on four-chamber glass slides were used for endocytosis analysis. Cells were incubated with 6.25 µL of Alexa Fluor 488-labeled Tf (Tf⁴⁸⁸) (5 mg/mL) in 500 µL of complete medium for different durations (from 1 minute to 4 hours). After removal of the media, cells were completely washed thrice using DPBS. Cells were then fixed with 10% neutralized formalin for 10 minutes and mounted for fluorescent microscopic observation. For immunocytochemical staining of TfR, cells were first fixed using 10% neutralized formalin for 10 minutes and then incubated with anti-TfR monoclonal antibody for 2 hours at room temperature. The antibody was prepared in DPBS with a dilution of 1:200. After DPBS washing (three times, 5 minutes each), cells were incubated with Alexa Fluor 588-labeled goat antimouse immunoglobulin G (Invitrogen) for 1 hour. Negative control was stained similarly except the anti-TfR antibody was replaced by DPBS.

Animal Models and Optical Imaging of Tumors

Two solid tumor xenograft models were developed by subcutaneous inoculation of 1×10^7 subconfluent cells of

JHU-013 in 100 μL of DPBS in the lower back or oral base tissues of athymic nude mice (8–10 weeks old; Harlan, Indianapolis, IN). Tumors were imaged when they reached certain sizes (2.4–9 mm in diameter). Fourteen tumors grown in the lower back of 12 mice, including 2 with tumors in both sides, were tested for the feasibility and fluorescent signal dynamics of Tf^{NIR} -based optical imaging. To verify the results, four tumors produced in the oral base tissues of four mice were further analyzed. Five healthy mice without tumors were used as the control.

Tf^{NIR} -based fluorescent optical imaging was performed using the IVIS 200 Imaging System (Caliper Life Sciences, Hopkinton, MA). Imaging and quantification of the signals were controlled by the acquisition and analysis software *Living Image* (Caliper Life Sciences). Mice were placed onto the warmed stage inside a light-tight camera box with continuous exposure to 2% isoflurane. Animals were given 200 μL (0.625 $\mu\text{g}/\mu\text{L}$) of the conjugate Tf^{NIR} through the tail vein. The entire animal was imaged every 10 to 30 minutes for at least 6 hours. The acquisition time for each image was 1 second. The light emitted from the mouse was detected, integrated, digitized, and displayed. Regions of interest from displayed images were identified and measured around the tumor sites. The signal intensity was expressed as mean flux (photons per second per centimeter squared per steradian, $\text{p/s}/\text{cm}^2/\text{sr}$). Contralateral leg muscle was selected as normal background.

Statistical Analysis

The tumor sizes were measured using calipers, and the relationship between fluorescent signal and tumor sizes was evaluated using the statistical software *OriginPro 7.0* (OriginLab, Northampton, MA). A significant correlation was inferred if a p value was $< .05$ by correlation analysis.

Results

Expression of TfR in HNSCC Cell Lines

To better understand the expression status of TfR in HNSCC, TfR levels were analyzed in four HNSCC cell lines and one normal squamous cell line. A significantly high expression level of TfR was detected in all four HNSCC cell lines compared with that in the normal squamous cell line (Figure 1, A and B). Immunocytochemistry further confirmed the expression of TfR in JHU-013 cells. An immunoreactive signal was clearly seen in the cell

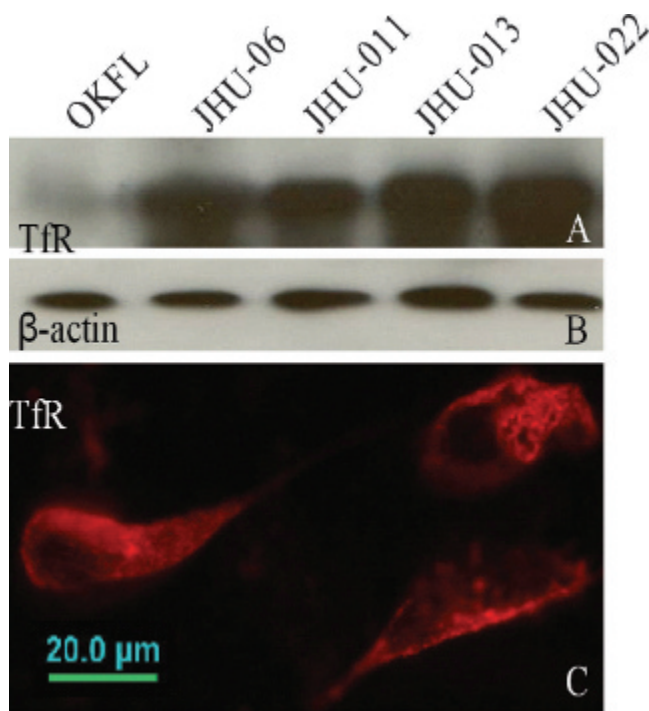


Figure 1. Transferrin receptor (TfR) expression. A, Western blot analysis of TfR expression showing overexpression of TfR in head and neck squamous cell carcinoma cell lines (JHU-06, 011, 013, 022) relative to that in a normal squamous cell line (OKFL). B, Same membrane re-probed with β -actin antibody. C, Immunocytochemistry in JHU-013 culture cells showing immunoreactive signal in cell membrane and cytoplasm.

membrane and cytoplasm (Figure 1C). Almost all of the tumor cells showed strong immunoreaction against TfR antibody. No signal was observed in the negative controls without primary antibody (data not shown).

Endocytosis and Exocytosis of Tf

The kinetics of endocytosis of Tf in JHU-013 cells was examined following incubation of fluorescence-labeled Tf (Tf^{488}) with monolayer cell cultures (Figure 2). Binding of Tf^{488} with TfR on the cell membrane was observed as early as 1 to 2 minutes after incubation. With prolonged incubation, Tf^{488} signal was seen in the cytoplasm and cell membrane. The maximum signal in the cytoplasm was observed after 1 to 2 hours of incubation, and the signal was distributed evenly within cytoplasm. With increased incubation time (3–4 hours), signal accumulation was observed in the regions surrounding the nuclei and regions close to the cell membrane. The total fluorescence decreased gradually thereafter, indicating exocytosis of Tf^{488} .

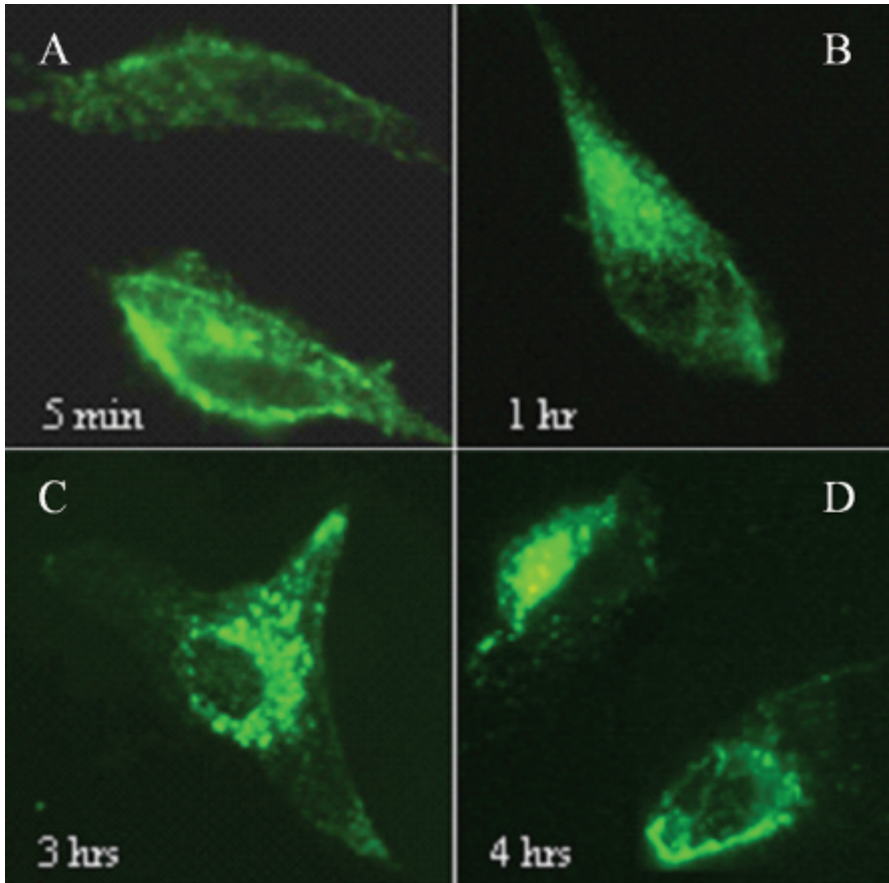


Figure 2. Different stages of transferrin (Tf) endocytosis. Cells were incubated with Tf for varied times and imaged, and representative images are presented. *A*, Tf signal mainly in cell membrane (5 minutes). *B*, Signal in both cell membrane and cytoplasm with an evenly distributed pattern (1 hour incubation). Signal mainly in the perinuclear area (*C*; 3-hour incubation) and the peripheral area (*D*; 4-hour incubation). Tf was labeled with Alexa Fluor 488. The original magnification was $\times 400$.

Tf^{NIR}-Based Tumor Imaging in Animal Models of Human HNSCC

The Tf^{NIR} conjugate contains 3 mol NIR fluorescent dye (Alexa Fluor 680)/mol Tf (Invitrogen). Two hundred microliters (0.625 $\mu\text{g}/\mu\text{L}$) of the Tf conjugate as a single bolus was administered via the tail vein of mice, and the whole animal was then imaged at different times. We first tested the imaging efficiency of Tf^{NIR} in human tumor xenografts ($n = 14$) grown in the lower back of athymic nude mice (Figure 3). The tumor sizes varied from 2.4 to 9 mm in diameter. A preferential accumulation of the fluorescence was detectable as early as 10 minutes in most tumors. The fluorescent signal in the tumors showed a rapid increase followed by a gradual decrease over time. The signal was still detectable after 48 hours. Interestingly, the time to reach the maximum fluorescence varied from 90 to 300 minutes, showing significant differences among tumors in different animals. In comparison with the tumor signal, the background fluorescence increased immediately after tail vein injection of the Tf^{NIR} and decayed much faster than tumor signal. The background fluorescence was observed mainly arising from the liver, bone marrow,

brain tissue, and spleen. The fluorescent signal intensity ($\text{p/s}/\text{cm}^2/\text{sr}$) was measured from the tumors and muscles in the opposite leg. The maximum tumor to muscle fluorescent signal ratio was reached within 6 hours in the majority of the tumors. The maximum ratio varied among tumors, ranging from 1.42 to 4.15. A positive correlation was observed between this ratio and the tumor sizes (2.4–9 mm in diameter) ($r = .74$, $p = .002$) (Figure 4).

To further test the *in vivo* imaging feasibility of Tf^{NIR} in HNSCC, tumor xenografts were also established in the oral base tissues in four mice (Figure 5). In healthy mice without tumor, the fluorescent signal was observed immediately in the neck and head following administration of Tf^{NIR}. The background fluorescent signal was observed arising mainly from the large blood vessels in the neck and brain tissue (Figure 5D). The background fluorescent signal was still detectable at 2 hours after injection. Importantly, in animals with tumors, although both background and tumor fluorescent signal were observed following injection, the background fluorescence decreased rapidly and was weak, whereas the tumor signal decreased slowly and was much stronger than background. The tumor in the oral base could be clearly imaged as those

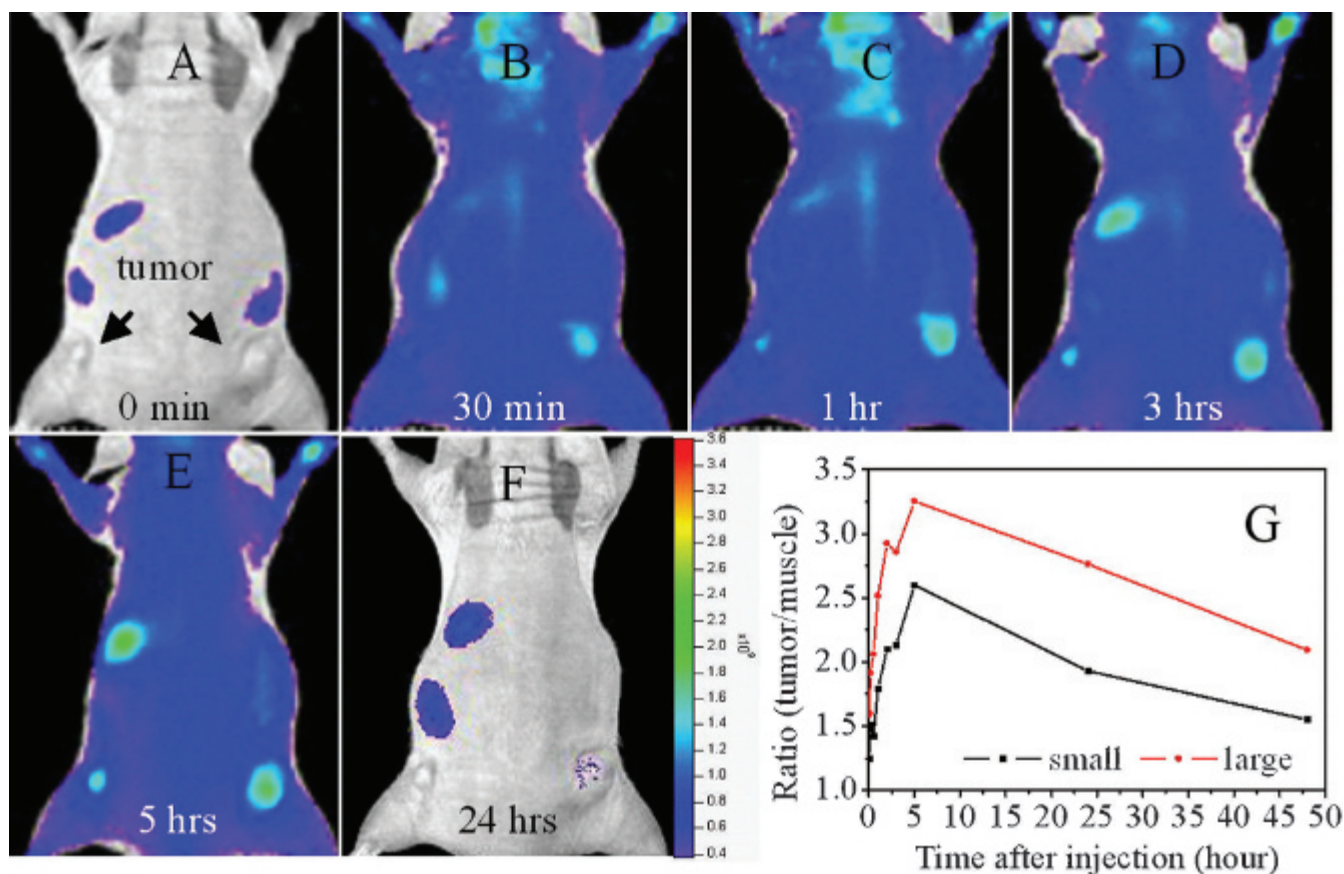


Figure 3. Whole-animal imaging following intravenous injection of near-infrared transferrin showing preferential accumulation of fluorescent signals in tumors. A to F show images taken at 0, 30 minutes, and 1, 3, 5, and 24 hours, separately. G shows change in the ratio of tumor to muscle fluorescence signal in small and large tumors over time.

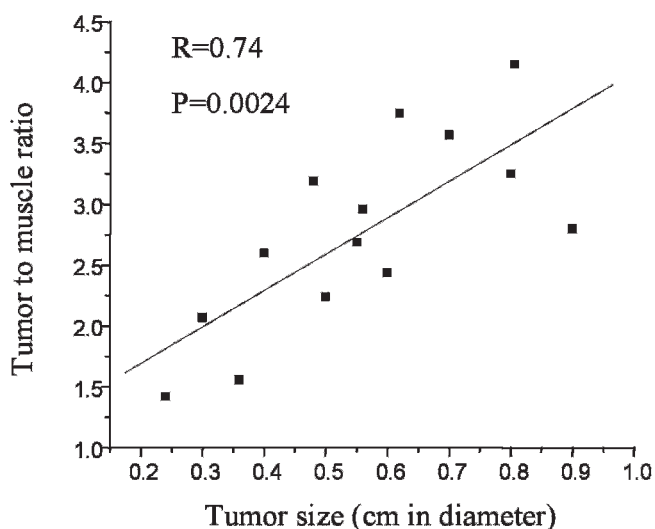


Figure 4. Positive correlation between the tumor size and the ratio of fluorescence signals from tumors to that from muscles.

in the lower back (Figure 5A–C). The background fluorescence appeared less problematic for detection of neck tumors owing to significantly weak intensity of the background compared with tumor signal.

Discussion

Theoretically, malignant tumor cells could be detected by imaging overexpressed biomarkers by taking advantage of specific binding of ligands with biomarkers and high sensitivity of optical imaging.^{1,3} Furthermore, optical assessment of the biomarker expression level is potentially helpful in assessment of tumor prognosis and drug sensitivity.^{21,22} Keeping these in mind, we tested the feasibility of tumor detection by targeted imaging of TfR using the fluorescent ligand Tf^{NIR}. TfR expression is found only in the basal layer of normal oral squamous epithelium at an extremely low level and is rarely detected in benign lesions.^{17–19} Importantly, TfR is expressed strongly in HNSCC, and a high expression level of TfR indicates high

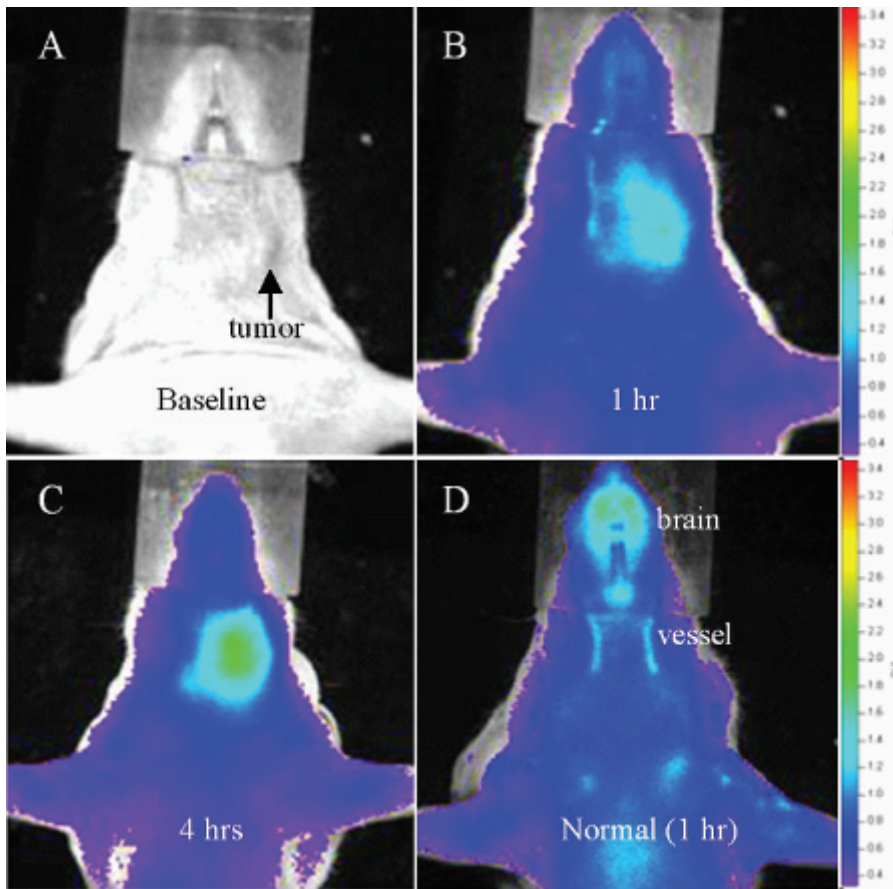


Figure 5. Near-infrared transferrin receptor (Tf^{NIR})-based imaging in healthy mice and mice with oral base tumor xenografts. A to C show images taken at 0, 1, and 4 hours, separately, following intravenous injection of Tf^{NIR} . Note the significant difference in fluorescence signals and kinetics of signal decay between tumors and background over time. D shows a healthy mouse with background signal from carotid arteries and brain tissue. The color intensity scale is the same for A, B, and C (minimum = 3.31×10^8 and maximum = 3.45×10^9). The color intensity scale for the healthy mouse in D is different (minimum = 3.83×10^8 and maximum = 2.59×10^9).

tumor malignancy and a poor prognosis.^{17–19} This specific expression pattern of TfR makes it an ideal candidate to image HNSCC. We hypothesized that the normal epithelia or benign lesions can be differentiated from malignant cells by exploring the differential expression of TfR. In the present study, overexpression of TfR was demonstrated in all HNSCC cell lines using Western blot analysis. Microscopic findings for the rapid binding of Tf^{NIR} with TfR and endocytotic activity of Tf^{NIR} in cell cultures further provided the rationale to image HNSCC in vivo using Tf^{NIR} . Specificity is critical for molecular imaging in vivo. Our previous work using MDA-MB-231 human breast cancer cells has shown that pretreatment of the cells with a threefold higher amount of unlabeled Tf ($375 \mu\text{g Tf/dish}$) than the probe ($125 \mu\text{g Tf}^{\text{NIR}}/\text{dish}$) resulted in a 66% decrease in the fluorescent signal.¹³ Specificity of the Tf moiety for targeting has also been demonstrated by other investigators.²³ In an in vitro study using $^{125}\text{I-Tf}$ in a K562 cell line, preincubation with 100-fold excess of unlabeled Tf for 5 minutes resulted in a dramatic inhibition of subsequent $^{125}\text{I-Tf}$ binding. A 100-fold excess of bovine serum albumin or asialo-orosomucoid (a glycoprotein) had no effect on $^{125}\text{I-Tf}$ binding.²³

To test our hypothesis, we first imaged HNSCC xenografts grown in the lower back of mice. Tf^{NIR} accumulated preferentially in the tumor xenografts. The maximum tumor signal to background ratio reached to 1.42 to 4.15 and could be observed within 6 hours in the majority of the tumors. The significantly high ratio enabled early detection of tumors with high sensitivity and specificity. Interestingly, the time to reach the highest signal in tumors varied among tumors and was not related to tumor sizes. This phenomenon is also observed in bioluminescent imaging following D-luciferin administration in tumors established with luciferase-expressing tumor cell lines (data not shown). The in vivo dynamic difference of Tf^{NIR} accumulation might be related to both animal individual and tumor characteristics such as tumor volume, tumor cell proliferation, vascular supply, and hypoxia.²⁴ The tumor fluorescent signal is a sum of photons from specific binding of the ligand with its receptor and nonspecific presence of the fluorescent conjugate in blood vessels and interstitial space. However, the nonspecific signal was cleared more rapidly than true tumor cell-bound signal and appeared less significant in tumor detection. Previous studies using

radiolabeled Tf showed a significant decrease in tumor signal by pretreatment with a large amount of unlabeled Tf.¹⁵ These results further indicate the importance and specificity of the Tf moiety for targeting *in vivo*. One major concern is the hypoxia and necrosis frequently presenting in large tumors.²⁵ Hypoxia and necrosis might affect both the expression of TfR and the entry, settling, and binding of Tf^{NIR}. These factors might become evident if quantitative assessment of biomarker expression or comparative analysis among tumors is performed using optical imaging, although we obtained a close correlation between the tumor to muscle fluorescent ratio and tumor size.

To further test the feasibility of HNSCC detection, we imaged the animals with and without oral base tumors. In healthy mice, fluorescent signal was observed from the large blood vessels in the neck and from brain tissue. The carotids and their branches and aorta arch are located superficially in the neck. Normal brain tissue is known to express TfR at a high level. The fluorescent background might adversely affect the detection of metastatic lesions in neck lymph nodes. Metastatic lesions might be too small to produce a stronger signal than the vessels in animal models (further study is necessary). Primary tumors can be clearly detected through the neck owing to a much stronger signal and delayed signal fading relative to background. Human HNSCC is developed and progressed through atypia to carcinoma *in situ* and then to invasive squamous cell carcinoma. These early lesions locate superficially in the wall of the oral cavity, pharynx, and esophagus. The difference in TfR expression among normal squamous epithelial cells, atypical cells, and carcinoma cells may be significant enough for optical differentiation among them through the use of Tf^{NIR}. Furthermore, development of confocal laser endomicroscopy enables analysis of *in vivo* microarchitecture.²⁶ The combination of a fluorescently labeled probe such as Tf^{NIR} and fluorescent confocal laser endomicroscopy will enable identification of early lesions, including squamous cell atypia and carcinoma *in situ*, as well as early invasive carcinomas. Our results in animal models of human HNSCC indicate that TfR is a promising target and Tf^{NIR}-based optical imaging is potentially useful for detection and localization of early HNSCC and atypical lesions in clinical practice.

Under physiologic conditions, iron-loaded Tf binds TfR on the surface of actively dividing cells. Subsequently, the Tf-TfR complex is internalized, first transported to early endosomes and then delivered to recycling endosomes. The apo-Tf is released only after the complex reaches the cell surface and then circulates until it again

comes in contact with free iron. It has been estimated that one Tf molecule could participate in this transport cycle as many as 100 times.²⁷ In the present study, the Tf was labeled with NIR fluorescent dye and the tumor was imaged based on the fluorescence of the optical reporter. The details of Tf^{NIR} recycling in tumors are unknown, and further analysis would be necessary for understanding the pharmacokinetics of Tf^{NIR} in mice.

References

1. Massoud TF, Gambhir SS. Molecular imaging in living subjects: seeing fundamental biological processes in a new light. *Gene Dev* 2003;17:545–80.
2. Graves EE, Weissleder R, Ntziachristos V. Fluorescence molecular imaging of small animal tumor models. *Curr Mol Med* 2004;4: 419–30.
3. Ntziachristos V, Bremer C, Weissleder R. Fluorescence imaging with near-infrared light: new technological advances that enable *in vivo* molecular imaging. *Eur Radiol* 2003;13:195–208.
4. Hogemann-Savellano D, Bos E, Blondet C, et al. The transferrin receptor: a potential molecular imaging marker for human cancer. *Neoplasia* 2003;5:495–506.
5. Stefflova K, Chen J, Zheng G. Using molecular beacons for cancer imaging and treatment. *Front Biosci* 2007;12:4709–21.
6. Hoffman RM. The multiple uses of fluorescent proteins to visualize cancer *in vivo*. *Nature* 2005;5:796–806.
7. Veiseh M, Gabikian P, Bahrami SB, et al. Tumor paint: a chlorotoxin: Cy5.5 bioconjugate for intraoperative visualization of cancer foci. *Cancer Res* 2007;67:6882–8.
8. Kaijzel EL, van der Pluijm G, Lowik CW. Whole-body optical imaging in animal models to assess cancer development and progression. *Clin Cancer Res* 2007;13:3490–7.
9. Greenlee RT, Hill-Harmon MB, Murray T, Thun M. Cancer statistics, 2001. *CA Cancer J Clin* 2001;51:15–36.
10. Forastiere A, Koch W, Trotti A, Sidransky D. Head and neck cancer. *N Engl J Med* 2001;345:1890–900.
11. Westra WH, Califano J. Toward early oral cancer detection using gene expression profiling of saliva: a thoroughfare or dead end? *Clin Cancer Res* 2004;10:8130–1.
12. Pirolo K, Dagata J, Wang P, et al. A tumor-targeted nanodelivery system to improve early MRI detection of cancer. *Mol Imaging* 2006;5:41–52.
13. Shan L, Wang S, Sridhar R, et al. A dual probe with fluorescent and magnetic properties for imaging solid tumor xenografts. *Mol Imaging* 2007;6:85–95.
14. Belloccq NC, Pun SH, Jensen GS, Davis ME. Transferrin-containing, cyclodextrin polymer-based particles for tumor-targeted gene delivery. *Bioconjug Chem* 2003;14:1122–32.
15. Smith TA, Perkins AC, Walton PH. 99mTc-labelled human serum transferrin for tumour imaging: an *in vitro* and *in vivo* study of the complex. *Nucl Med Commun* 2004;25:387–91.
16. Vavere AL, Welch MJ. Preparation, biodistribution, and small animal PET of 45Ti-transferrin. *J Nucl Med* 2005;46:683–90.
17. Miyamoto T, Tanaka N, Eishi Y, Amagasa T. Transferrin receptor in oral tumors. *Int J Oral Maxillofac Surg* 1994;23:430–3.

18. Kearsley JH, Furlong KL, Cooke RA, Waters MJ. An immunohistochemical assessment of cellular proliferation markers in head and neck squamous cell cancers. *Br J Cancer* 1990;61:821–7.
19. Tanaka N, Miyamoto T, Saito M, et al. Transferrin receptor expression in oral tumors. *Bull Tokyo Med Dent Univ* 1991;38:19–26.
20. Dickson M, Hahn W, Ino Y, et al. Human keratinocytes that express hTERT and also bypass a p16INK4a-enforced mechanism that limits life span become immortal yet retain normal growth and differentiation characteristics. *Mol Cell Biol* 2000;20:1436–47.
21. Klausner RD, Renswoude JV, Ashwell G, et al. Receptor-mediated endocytosis of transferrin in K562 cells. *J Biol Chem* 1982;258:4715–24.
22. Zhang W, Moorthy B, Chen M, et al. A Cyp1a2-luciferase transgenic CD-1 mouse model: responses to aryl hydrocarbons similar to the humanized AhR mice. *Toxicol Sci* 2004;82:297–307.
23. Pillon A, Servant N, Vignon F, et al. *In vivo* bioluminescent imaging to evaluate estrogenic activities of endocrine disrupters. *Analyt Biochem* 2005;340:295–302.
24. Raman V, Artemov D, Pathak AP, et al. Characterizing vascular parameters in hypoxic regions: a combined magnetic resonance and optical imaging study of a human prostate cancer model. *Urol Oncol* 2007;25:358–9.
25. Kanematsu M, Semelka R, Osada S, Amaoka N. Magnetic resonance imaging and expression of vascular endothelial growth factor in hepatocellular nodules in cirrhosis and hepatocellular carcinomas. *Top Magn Reson Imaging* 2005;16:67–75.
26. Hoffman A, Goetz M, Vieth M, et al. Confocal laser endomicroscopy: technical status and current indications. *Endoscopy* 2006;38:1275–83.
27. Gomme PT, McCann KB, Bertolini J. Transferrin: structure, function and potential therapeutic actions. *Drug Discov Today* 2005;10:267–73.